Dominant Effect of Protein Charge Rather Than Protein Shape in Apparent DNA Bending by Engineered bZIP Domains†

Philip R. Hardwidge,‡ Jason D. Kahn,§ and L. James Maher, III*,‡

Department of Biochemistry and Molecular Biology, Mayo Foundation, Rochester, Minnesota 55905, and Department of Chemistry and Biochemistry, University of Maryland, College Park, Maryland 20742-2021

Received March 5, 2002

ABSTRACT: We are interested in how asymmetric charge neutralization of DNA by proteins results in DNA bending. We have previously reported electrophoretic phasing experiments utilizing homodimer peptides derived from GCN4, a yeast basic zipper (bZIP) transcription factor. Here we report the results of experiments that examine the importance of peptide sequence context in DNA bending and test the hypothesis that peptide structural asymmetry causes electrophoretic anomalies in the absence of DNA bending. We prepared two new series of bZIP peptides that differed dramatically in overall size, structure, and peptide sequence near the DNA. The magnitude of apparent DNA bending is independent of the structure of the protein. This result reduces the concern that bZIP protein structure causes electrophoretic anomalies in the absence of DNA bending. In all cases, both the magnitude and direction of the apparent DNA bend angle are strongly dependent on the local peptide charge. We attempted to validate independently our results with a minicircle competition binding assay. Binding preferences of severalfold for properly phased circular versus linear DNA templates were predicted. However, no binding preferences were observed. We propose that the minicircle binding assay may be intrinsically insensitive to DNA bending or flexibility induced by the bZIP peptides studied, and we provide a unifying explanation for the discrepancies between the cyclization and electrophoretic experiments.

Protein-mediated DNA bending is important to many fundamental cellular processes including DNA compaction into nucleosomes (*1*), the assembly of transcriptionally active nucleoprotein complexes (*2*), and recombination (*3*). In dilute solution, DNA has a persistence length of ∼150 bp, making the polymer locally stiff but globally flexible. Free energy release upon protein binding can be sufficient to drive DNA bending into compact, folded structures (*4*, *5*).

We have been interested in the mechanism of DNA bending by proteins that contact DNA through electrostatic interactions between cationic amino acids and the DNA sugar−phosphate backbone. It has been hypothesized that certain cationic amino acid side chains interact with the DNA backbone in such a way as to screen fully certain DNA phosphate charges from one another. Such screening is proposed to cause an asymmetric decrease in local phosphate−phosphate charge repulsions on the protein-bound face of the helix relative to the face away from the protein, where counterion condensation leaves a residual negative charge at each phosphate (*6*). The resulting unbalanced interphosphate repulsions are predicted to cause a collapse of the DNA backbone toward the protein (*7*). Although important energetic contributions to DNA bending are undoubtedly made by other features of the protein−DNA interface, our laboratory has been investigating whether the hypothetical charge collapse of the DNA backbone plays a significant role (*8*−*11*).

The dimeric DNA-binding domain of transcription factor GCN4 forms a basic leucine zipper (bZIP) motif by which GCN4 binds regulatory elements upstream of yeast amino acid biosynthesis genes (Figure 1A). Apparent DNA bending by charge variants of this bZIP domain has been studied previously by our laboratory (*10*, *12*). Others have examined DNA bending by related bZIP proteins (*13*−*15*). Three amino acids immediately N-terminal to the basic region of each ∼70 amino acid bZIP monomer reside close to the DNA helix (*16*; Figure 1B). Kerppola (*17*) and Schepartz (*14*) noted that the presence of charged residues in these positions correlates strongly with apparent DNA bending in the resulting protein−DNA complexes, as measured by electrophoretic phasing assays. Examination of the crystal structure of the GCN4 bZIP−DNA complex shows little deformation of the AP-1 DNA-binding site (*16*). Since GCN4 contains a neutral amino acid cluster (PAA) immediately N-terminal to the basic region, the absence of DNA bending is consistent with DNA bending models from electrophoretic assays.

We reasoned that if interphosphate repulsions help to determine DNA shape, substitution of cationic or anionic amino acids for the neutral amino acids (PAA) of the GCN4 bZIP would result in DNA bending in different directions. Results of our previous electrophoretic phasing analyses supported this hypothesis: cationic amino acid substitutions resulted in an apparent DNA bend toward the positive charges, while anionic amino acid substitutions caused apparent DNA bending away from the negative charges (*10*, *14*). Similar results were reported with complexes involving variants of the bZIP domains of Jun and Fos (*13*).

† This work was supported by the Mayo Foundation and NIH Grant GM54411 to L.J.M.

* To whom correspondence should be addressed. Tel: (507) 284-9041. Fax: (507) 284-2053. E-mail: maher@mayo.edu.

‡ Mayo Foundation.

§ University of Maryland.

10.1021/bi020185h CCC: $22.00
Published on Web 06/05/2002

Electrophoretic phasing assays systematically rotate the recognition sequence of a DNA-binding protein relative to a fixed element of DNA curvature provided by an array of A_{5-6} tracts. If the bound protein causes a DNA bend, each complex will have a different overall shape and electrophoretic mobility. Although they provide DNA bending estimates consistent with other techniques for well-studied globular proteins such as *Escherichia coli* CAP[1] (*18*), gel-based methods have limitations. One cannot from first principles predict the relationship between molecular shape and mobility through a gel matrix. Analyses rely on empirical calibrations of electrophoretic behavior and the assumption that the reduced mobility of bent DNA relative to straight DNA is due to the corresponding reduction in end-to-end distance. It must also be assumed that the shape of the DNA in a protein−DNA complex dominates the electrophoretic properties of the complex (*15*). Recent studies of bZIP−DNA complexes have raised concerns that either the extended shape of the leucine zipper domain or differences in the rigidity of the protein−DNA complex may influence the electrophoretic properties of the complex (*19*).

Conflicting results between gel- and solution-based methods have been obtained for derivatives of the bZIP heterodimer Fos-Jun. Electrophoretic phasing assays suggest that Fos-Jun derivatives induce a 15−30° bend in the DNA double helix (*20*, *21*), whereas crystal structures, cyclization kinetics, and minicircle competition binding assays indicate that various related Fos-Jun derivatives do not bend DNA (*15*, *19*). Although some of this discrepancy may be due to inconsistency in the particular peptide constructs tested (*22*), electrophoretic phasing assays have been questioned in the analysis of DNA bending by bZIP proteins (*15*, *19*).

Our previous experiments utilized identical bZIP domains in which only three amino acids were varied to produce charge variants (*10*). An electrophoretic phasing anomaly was not observed with the neutral variant (PAA). This result clearly demonstrates that the relative orientation of the extended leucine zipper domain has no effect on electrophoretic mobility with these DNA probes. Nonetheless, it remains possible that the large phasing-dependent mobility differences observed for charge variants are due to some charge-dependent property other than DNA bending, perhaps differential flexibility of the protein−DNA interface among charge variants (*15*). We have therefore initiated several independent approaches to corroborate electrophoretic phasing data that suggest DNA bending by bZIP charge variant proteins.

Here we report the results of experiments that test the hypothesis that the inherent structural asymmetry of the elongated bZIP domain can cause charge-dependent electrophoretic anomalies in the absence of DNA bending. To each N-terminus of an ~70 amino acid bZIP monomer we now fuse the 366 amino acid globular domain of the maltose binding protein (MBP; Figure 1C). Examination of the individual crystal structures of the GCN4 bZIP domain and MBP suggests that such fusions would create protein−DNA complexes that are roughly symmetrical in the degree of protein extension away from opposite faces of the DNA. If electrophoretic anomaly is a result of leucine zipper conformation or flexibility, we hypothesized that different mobility effects would be expected for MBP-bZIP fusions. We report electrophoretic results that do not support this hypothesis. For MBP-bZIP fusions, the electrophoretic mobilities of peptide−DNA complexes again depend strongly upon the electrostatic character of the amino acids adjacent to the DNA, as previously observed for bZIP peptides without pendant MBP domains. Overall, a roughly linear correlation between the apparent DNA bend angle and the peptide charge is observed for all peptides studied. The independence of this result from the presence or absence of the large globular MBP domain makes it more difficult to invoke the asymmetry of the leucine zipper as the source of the charge-dependent electrophoretic anomaly. Additional experiments varied the charge of the entire linker domain between MBP and the bZIP domain. The results of these experiments also support the same electrostatic model for DNA bending by bound bZIP proteins.

DNA bending proteins should, in theory, display an affinity preference for properly constructed DNA minicircles relative to linear DNA (*15*). The expected binding enhancement has been observed for TBP and CAP, two proteins that induced large DNA bends (*23*, *24*). We report Monte Carlo simulations to predict the effect of DNA bending, of the magnitude suggested by our electrophoretic work, on the predicted ring closure efficiencies of phasing constructs bearing the AP-1 site. These results then give the corresponding binding preferences for circular vs linear DNA probes. Differential affinities of ~2−3-fold for properly phased circular DNA vs linear DNA were predicted among probes bound to bZIP charge variants. In contrast to this prediction, minicircle binding assays did not detect a differential affinity for circular vs linear DNA for any bZIP charge variant studied. Therefore, despite the consistency of our electrophoretic phasing results, we report discordant results of minicircle binding assays. We propose that the minicircle binding assay may be intrinsically insensitive to DNA bending or flexibility induced by the bZIP peptides studied, and we provide a unifying explanation for the discrepancies between the cyclization and electrophoretic experiments.

MATERIALS AND METHODS

Preparation of bZIP Charge Variants. Initial T7-XXX peptides were charge variants of the bZIP domain derived from GCN4, expressed as crude *E. coli* cell lysates (Table 1; *10*). PCR and standard subcloning methodologies were used to modify the N-terminus of the T7-XXX peptides by appending a hexahistidine tag to create the indicated His-XXX peptides (Table 1). His-XXX peptides were purified on Ni^{2+}-NTA−agarose columns to greater than 90% homogeneity (*25*). The pMAL-c2X vector system (New England Biolabs, Beverly, MA) was used to create fusions between the 366 amino acid maltose binding protein (MBP), encoded by the *E. coli malE* gene, and the ~70 amino acid bZIP domain of GCN4. These protein fusions are designated as MBP-bZIP fusions (Table 1). MBP-bZIP fusions were purified by amylose affinity chromatography under native conditions according to the manufacturer's instructions (New England Biolabs, Beverly, MA). In all cases, protein purity was confirmed by Coomassie staining of 10% Bis-Tris acrylamide gels (Novex). DNA-binding activity was determined by standard gel-shift methods.

[1] Abbreviations: CAP, *Escherichia coli* catabolite activator protein; FRET, fluorescence resonance energy transfer; MBP, maltose binding protein; TBP, TATA box binding protein.

Electrophoretic Phasing Analyses. Probes for electrophoretic phasing analysis were prepared by PCR from plasmids pDP-AP-1-21, -23, -26, -28, and -30 as previously described (*10*, *26*). Pairs of curved DNA standards containing different numbers of phased A_6 tracts at either the center or one terminus of each fragment were prepared by digestion of plasmids pJT170-2 through pJT170-9 with either *Nhe*I or *Bam*HI (*27*). The resulting ~440 bp duplex DNA fragments were purified and radiolabeled as previously described (*10*). Binding studies were performed by incubation of the indicated peptide (~5 nM) with ~100 pM radiolabeled duplex DNA probes (AP-1-21, -23, -26, -28, or -30; see above) in a final reaction mixture of 10 μL containing 10 mM HEPES, pH 8.0, 20 mM NaCl, 10% glycerol, 1 mM EDTA, 1 mM DTT, 0.05% Triton X-100, and 15 ng/μL poly(dI·dC). Solutions were incubated on ice for 30 min. Free and protein-bound DNA probes were resolved by native 8% polyacrylamide gel electrophoresis (29:1 acrylamide:bisacrylamide) in 0.5× TBE buffer for 20 h at 4 °C (12 V/cm). Dried gels were analyzed by storage phosphor technology. Phasing calculations were performed as previously described (*10*). In these experiments, the factor used to correct for electrophoresis conditions, *k* (*28*), was determined to be 1.16 ± 0.01. The phasing data suggest that estimated DNA bend angles can be interpreted as being toward the major or minor groove viewed at the center of the AP-1 site. This interpretation is reasonable, as both the protein and DNA are locally symmetric about this position.

Monte Carlo Simulation of the Effect of Peptide-Induced DNA Bending on DNA Cyclization. Monte Carlo simulations were performed to calculate the *J* factors (effective DNA end concentrations) for cyclization of 156 bp DNA fragments bearing A tracts and AP-1 sites (*15*). These results were used to calculate the predicted linear/circular binding affinity ratios according to the quasi-thermodynamic cycle relating cyclization and binding: the ratio of *J* factors for any two molecules should be equal to K_{rel} (see eq 1) for the two (*24*). Simulations were performed essentially as described (*29*), using programs adapted from previous work in the Crothers group (*30*, *31*). Briefly, 10^5 DNA half-chains are constructed, each one by adding vectors representing the helix axis to generate the chain. The rotation matrices relating the helix axis and the twist of one base pair relative to the previous one are generated using Gaussian distributions for roll, tilt, and twist angles. Simulation parameters were *P* (persistence length) = 463 Å, *C* (torsional modulus) = 2.0×10^{-19} erg·cm, and helical repeat 10.45 bp/turn throughout, except 10.33 bp/turn in A tracts. All results reported here used the junction model for A tract DNA with 18° of bending per A tract. Parallel simulations using a wedge angle model (*32*) scaled to 18° per A tract, which models bending of mixed-sequence DNA outside the A tracts, gave qualitatively similar results but predicted larger binding preferences. Protein-induced DNA bends were represented as 20° kinks by roll, with half of the bend on each side of the central base pair of the site. No allowance was made for protein-induced stiffening or flexure, which would tend to increase or decrease the predicted effects, respectively. Full chains were generated by pairwise combinations of all the half-chains and *J* factors determined as described (*29*). Predicted values for K_{rel} are then given by *J* (−bend)/*J* (+bend) for each phasing construct. Error estimates are based on repeated simulations, which are reproducible to about 20%. *J* factors ranged from 30 to 500 nM, well within the range where these methods are believed to be reasonably precise.

Minicircle Competition Assays. Minicircle probes were prepared by PCR from templates kindly provided by Dr. Ayesha Sitlani (*15*). Minicircle probes were purified essentially as described (*15*). Briefly, PCR products were digested overnight with *Cla*I and purified by centrifugal gel filtration. Minicircle probes were also alternatively subcloned into a pGEM-Teasy vector (Promega), restricted with *Cla*I, end-labeled with [γ-^{32}P]ATP and T4 polynucleotide kinase, and gel-purified. One-half of the radiolabeled product was incubated overnight with T4 DNA ligase, while the other half was left untreated. Unligated (linear) and ligated (circular) probes were subsequently purified on native polyacrylamide gels. Circular vs linear assignments were confirmed by enzymatic characterization with *Cla*I and *Bal*31 exonuclease. Linear and circular probe concentrations (cpm) were equalized prior to protein binding experiments. Protein concentrations were adjusted empirically to shift approximately 50% of each probe. Preliminary experiments that altered the order of addition of linear and circular probes demonstrated that binding reactions had reached equilibrium after 30 min of incubation. Protein was incubated on ice for 30 min with equal amounts of linear and circular probes in 10 μL reactions containing 10 mM HEPES, pH 8.0, 20 mM NaCl, 10% glycerol, 1 mM EDTA, 1 mM DTT, 0.05% Triton X-100, and 15 ng/μL poly(dI·dC), followed by the addition of 2 μL of native gel loading buffer. Reactions were electrophoresed at 250 V on 5% polyacrylamide gels (29:1 acrylamide:bisacrylamide) for 5 h at 4 °C and exposed to a storage phosphor screen for 24 h. Data were analyzed with a Storm 840 PhosphorImager. The amount of free probe and probe bound by protein was determined independently for the linear and circular probes. Binding preference (K_{rel}) for linear vs circular probes was computed according to

$$K_{rel} = \left(\frac{\text{circle}_{free}}{\text{circle}_{bound}}\right)\left(\frac{\text{linear}_{bound}}{\text{linear}_{free}}\right) \quad (1)$$

where subscripts bound and free refer to radiolabeled DNA probes (circular and linear forms) complexed or free from peptide, respectively.

RESULTS

Experimental Rationale. We have previously utilized electrophoretic phasing assays to test DNA bending by bZIP charge variants (*10*, *33*). We have focused on electrostatic interactions between the DNA sugar−phosphate backbone and nearby amino acids. Due to controversy surrounding the interpretation of electrophoretic phasing assays utilizing proteins with nonglobular shapes (*19*), we and others have sought independent approaches to test hypotheses regarding the effect of local charge asymmetry on DNA conformation (*15*, *25*).

Of concern is the potential for the extended leucine zipper domains in bZIP and b-HLH-ZIP proteins to contribute to anomalous electrophoretic mobility, independent of DNA bending (*15*, *34*). This hypothesis has not been directly tested. To address aspects of this issue, we have created a family of fusion proteins in which the 366 amino acid globular *E. coli* maltose binding protein (MBP) is fused upstream of the

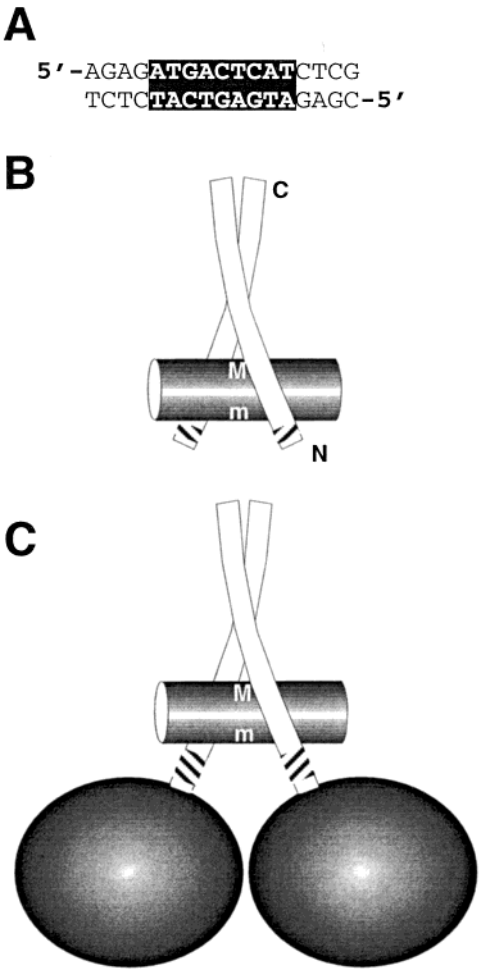

FIGURE 1: Schematic illustrations of bZIP peptides and DNA duplexes under investigation. (A) AP-1 DNA sequence recognized by GCN4 derivatives. The consensus binding site is shown in white letters, in the sequence context present, within 437−446 bp electrophoretic phasing probes. (B) Binding of bZIP homodimer (white; N- and C-termini indicated) to the AP-1 DNA sequence (gray tube), based on the published crystal structure (*16*). Peptide sequences and designations are listed in Table 1. Besides the sequences shown in Table 1, all depicted bZIP peptides contain an identical set of 52 additional amino acids at the C-terminus (Table 1, legend). Stripes indicate the location of charge variants. M and m indicate the major and minor grooves, respectively, at the center of the AP-1 site. (C) Model of MBP-bZIP protein fusions bound to the AP-1 DNA sequence. MBP domains (366 amino acids) are shown as gray spheres, depicted to scale according to a published crystal structure (*35*). Stripes indicate the linker domain location of charge variants.

∼70 amino acid bZIP domain of GCN4. On the basis of the crystal structures of the domains, we concluded that the extended leucine zipper would no longer be the dominant feature of the overall shape of such protein−DNA complexes. Appendage of the MBP domain to the N-terminus of each bZIP monomer increases the approximate size of the resultant protein dimer from ∼16 to 91 kDa.

Figure 1 illustrates this model system. Figure 1A highlights the consensus AP-1 site to which the proteins bind in electrophoretic phasing assays. The bZIP domain of GCN4 bound to AP-1 DNA is depicted in Figure 1B (*16*), and a schematic representation (approximately to scale based on crystal structures) of the MBP-bZIP fusion proteins that we created is illustrated in Figure 1C (*16*, *35*). The illustration demonstrates that the leucine zipper is no longer the dominant structure. The locations of charge variations are indicated by stripes (Figure 1B,C).

Protein Expression and Characterization. The proteins and nomenclature used in these experiments are presented in Table 1. T7-XXX peptides refer to bZIP charge variants described previously (*10*). The position of the variable amino acid cluster is in bold at the C-terminal end of the depicted sequences (Table 1). His-XXX peptides were constructed to modify the amino-terminal amino acid context of T7-XXX peptides and append a hexahistidine tag (Table 1). MBP-bZIP fusion peptides (Table 1) were created by subcloning the DNA-binding domains of bZIP charge variants (His-XXX peptide context) into the pMAL fusion system. An additional series of MBP peptides that altered the electrostatic character of the linker between MBP and the GCN4 bZIP DNA-binding domain was also created (Table 1). Specific binding of all peptides to the AP-1 site was demonstrated by gel-shift analysis.

Apparent DNA Bending by bZIP Charge Variants in Electrophoretic Phasing Assays. Electrophoretic phasing was employed to measure changes in DNA probe mobility due to the binding of bZIP charge variant peptides. Phasing probes (∼440 bp) contained an array of A_{5-6} tracts located at different distances from the AP-1 sequence (*10*). If peptide binding causes DNA bending, different mobilities are observed with changes of the helical phasing between the two elements (reference A_{5-6} tracts vs peptide bound to the AP-1 site). When curved loci are aligned in cis, gel mobility is minimized. The extent to which gel mobility is reduced in each probe is interpreted as a measure of the DNA bend angle and direction caused by peptide binding.

Our strategy was to collect apparent DNA bending data for bZIP charge variants in different amino acid sequence contexts and then analyze the data to discern if a dominant electrostatic effect persisted independent of peptide sequence context. Changes in DNA electrophoretic mobility induced by MBP-bZIP fusions were assayed for comparison with other bZIP peptides. In these experiments, the exact orientation of the MBP domain is unknown, but it is assumed to lie on the opposite side of the DNA from the leucine zipper domain. Overall, we observed that all three of the MBP-bZIP fusions bend DNA toward the major groove, but to very different extents. The highest degree of bending was induced by MBP-EEE and the lowest degree by MBP-KKK.

Example phasing data are shown in Figure 2A. Lanes 1−5 display the mobilities of complexes involving the binding of MBP-PAA (Table 1) to the phasing probes. Different phasings between the three reference A_{5-6} tracts and the occupied AP-1 site result in substantial mobility differences among the bound probes. Mobility retardation is maximal for probe pDP-AP-1-26 (Figure 2A, lane 3), where the center of the AP-1 site is most nearly in phase with A-tract curvature. Mobility retardation is minimized in probes pDP-AP-1-21 and -30 (Figure 2A, lanes 1 and 5), where the loci of curvature are out of phase. Similar results had been observed in our previous studies with T7 peptides and provided evidence of bending of the AP-1 site toward the major groove, i.e., *away from* anionic amino acids in the bZIP peptides (*10*; Figure 1B). Because the PAA sequence in MBP-PAA is not itself acidic, this result raised the possibility that the acidic context for PAA in MBP-PAA was important.

Table 1: Peptides Used in Electrophoretic Phasing Assay

Designation[a]	Sequence[b]	Tripeptide charge[c]	N-terminal charge[d]
T7-PAA	MASMTGGQQMGRD**PAA**...	0	0
T7-PAE	MASMTGGQQMGRD**PAE**...	−2	−2
T7-PEE	MASMTGGQQMGRD**PEE**...	−4	−4
T7-EEE	MASMTGGQQMGRD**EEE**...	−6	−6
T7-PAK	MASMTGGQQMGRD**PAK**...	+2	+2
T7-PKK	MASMTGGQQMGRD**PKK**...	+4	+4
T7-KKK	MASMTGGQQMGRD**KKK**...	+6	+6
His-PAA	MRGSHHHHHHRSMGRD**PAA**...	0	+4
His-PAE	MRGSHHHHHHRSMGRD**PAE**...	−2	+2
His-PEE	MRGSHHHHHHRSMGRD**PEE**...	−4	0
His-EEE	MRGSHHHHHHRSMGRD**EEE**...	−6	−2
His-PAK	MRGSHHHHHHRSMGRD**PAK**...	+2	+6
His-PKK	MRGSHHHHHHRSMGRD**PKK**...	+4	+8
His-KKK	MRGSHHHHHHRSMGRD**KKK**...	+6	+10
MBP-PAA	(MBP)-S_3N_{10}LGIEGRISEFPESSD**PAA**...	0	−6
MBP-EEE	(MBP)-S_3N_{10}LGIEGRISEFPESSD**EEE**...	−6	−12
MBP-KKK	(MBP)-S_3N_{10}LGIEGRISEFPESSD**KKK**...	+6	0
MBP-K_{10}-PAA	(MBP)-S_3N_{10}LGIEGRISEL**KKKKKKKKKK**QFPESSDPAA...	0	+14
MBP-E_{10}-PAA	(MBP)-S_3N_{10}LGIEGRISEL**EEEEEEEEEE**QFPESSDPAA...	0	−26
MBP-$(KE)_5$-PAA	(MBP)-S_3N_{10}LGIEGRISEL**KEKEKEKEKE**QFPESSDPAA...	0	−6
MBP-$(GS)_5$-PAA	(MBP)-S_3N_{10}LGIEGRISEL**GSGSGSGSGS**QFPESSDPAA...	0	−6
MBP-$(GK)_8$-PAA	(MBP)-S_3N_{10}LGIEGRISEL**GKGKSKSKGKSKSKGK**FPESSDPAA...	0	+10
MBP-$K_{10}(GS)_5$-PAA	(MBP)-S_3N_{10}LGIEGRISEL**KKKKKKKKKKGSGSGSGSGS**QFPESSDPAA...	0	+14

[a] Domains are separated by hyphens. T7-, His-, and MBP- designations indicate alternate leader sequences. MBP is 366 amino acids. [b] Residues in bold indicate charge variants. All peptides contain the additional C-terminal sequence -LKRARNTEA_2R_2SRARKLQRMKQLEDKVE_2L_2SKNYHLENEVAELK$_2$LESGQ encoding the basic and leucine zipper domains. [c] Formal amino acid charge in the mutagenized tripeptide region of the dimer (the three C-terminal residues of column 2). Obtained by counting −1 for D and E residues and +1 for K and R residues and multiplying the result by 2 for the dimer. At pH 8.0−8.3, histidine residues are uncharged. [d] Formal amino acid charge in the entire linker region of the dimer, excluding MBP. Charge assignments were identical to those described in footnote *c*.

Mobility anomaly differences are amplified as the charge of the amino acid cluster in the MBP-PAA dimer is decreased from 0 to −6. Thus, relative to MBP-PAA (Figure 2A, lanes 1−5), mobility differences of DNA probes bound by MBP-EEE (Figure 2A, lanes 6−10) were more pronounced. The probe pDP-AP-1-26 was again the most retarded in the gel, suggesting that the direction of DNA bending is similar in MBP-PAA and MBP-EEE complexes. In contrast, a different profile of AP-1 probe mobilities was seen in complexes with the cationic variant MBP-KKK (Figure 2A, lanes 11−15). In this case, mobility differences are greatly reduced, suggesting that bending toward the major groove at the center of the AP-1 site is much reduced in the presence of added cationic amino acids near DNA. This result again suggests that the balance of charge in the context of the MBP-bZIP fusion is reflected in the DNA bend angle.

The gel mobility measurements of each complex were transformed as described previously (*10*). Relative mobility was plotted against the distance in base pairs between the center of the AP-1 site and the center of curvature in the three phased A_{5-6} tracts. The results are depicted in Figure 2B. Using techniques derived by Kerppola and co-workers (*28*), the relative differences in probe mobilities were transformed into estimates of DNA bend magnitude and direction due to peptide binding.

Estimated DNA bend angles were derived from comprehensive phasing experiments for the T7- XXX, His-XXX, and MBP-bZIP fusion peptides shown in Table 1. Positive and negative bend angles refer to apparent DNA bending at the center of the AP-1 site toward the minor or major grooves, respectively. In all cases, the best estimate for the bend direction was toward the indicated groove, viewed in a reference frame within ∼0.5 bp 3′ from the center of the AP-1 site. Bending data were plotted against the total tripeptide charge (Table 1, column 3) of the dimer (Figure 3). The results indicate similar approximately linear relationships between the DNA bend angles and the tripeptide charge for the dimeric T7-XXX, His-XXX, and MBP-bZIP fusion peptides. Within the T7-XXX and His-XXX peptide series, apparent DNA bending is in opposite directions for highly anionic (EEE) vs cationic (KKK) peptides. Apparent DNA bend angles induced by MBP-bZIP fusions display an upward shift (Figure 3). However, the curves in Figure 3 remain evenly spaced, suggesting a striking and constant underlying electrostatic effect on DNA bending. The similar slopes of these curves even in the presence of the dramatically different N-termini of T7-XXX, His-XXX, and MBP-bZIP fusion peptides argue against a dominant role for protein structure in causing apparent DNA bending.

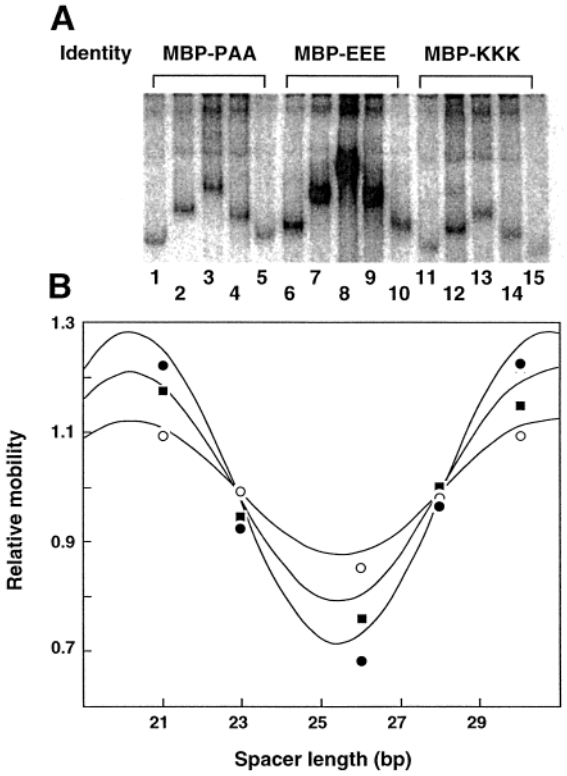

FIGURE 2: Electrophoretic phasing assays of apparent DNA bending by MBP-bZIP fusions. (A) Electrophoretic mobility shift assay of MBP-bZIP charge variants bound to phasing analysis probes. Each set of five lanes shows phasing probes derived from plasmids pDP-AP-1-21, -23, -26, -28, and -30, respectively (*12*, *26*), incubated with the MBP-bZIP fusions MBP-PAA (lanes 1−5), MBP-EEE (lanes 6−10), and MBP-KKK (lanes 11−15). (B) Analysis of phasing data. The relative mobility of each of the five phasing probes in a given protein complex is plotted as a function of the spacing (bp) between the center of the AP-1 site and the center of the A_{5-6} tract array, as described (*10*, *28*). Relative mobilities of complexes involving MBP-PAA (filled squares), MBP-EEE (filled circles), and MBP-KKK (open circles) are shown. The gel mobility measurements of each complex were transformed as described previously (*10*).

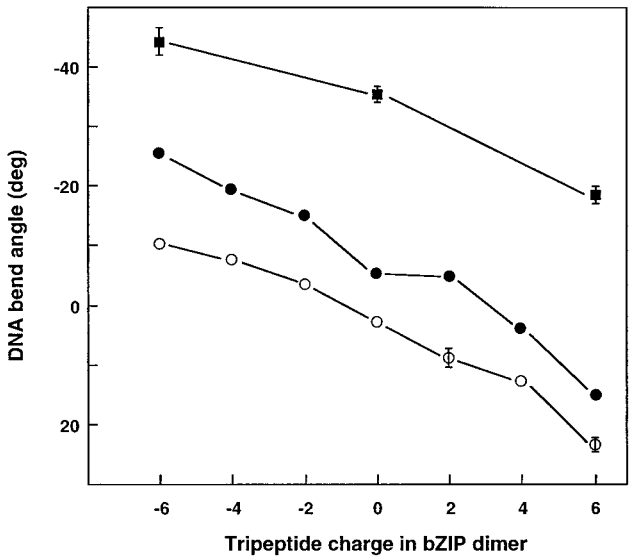

FIGURE 3: Correlation between apparent DNA bend angle and tripeptide charge in the dimer. The apparent DNA bend angle estimated from electrophoretic phasing experiments is plotted against the formal charge in a mutagenized tripeptide cluster of bZIP charge variants derived from GCN4. Data for peptides bearing N-termini designated MBP (filled squares), T7 (filled circles), and His (open circles) are shown (see Table 1). Apparent DNA bend angles are shown such that negative values indicate apparent bending toward the zipper (narrowing the major groove and widening the minor groove at the center of the AP-1 site). Positive values indicate apparent DNA bending away from the zipper (widening the major groove and narrowing the minor groove at the center of the AP-1 site). Data are shown as the mean and standard deviation of at least three independent experiments. Error bars are not shown when smaller than the symbols used.

The data in Figure 3 consider only the charge of the three varied amino acids at the positions occupied by PAA in the bZIP peptide (bold in the second column of Table 1). Full consideration of N-terminal amino acid charges near DNA yields the formal dimer charge assignments shown in the right column of Table 1. We hypothesized that the different vertical displacements of curves in Figure 3 could reflect the overall charge context of these three different peptide series. Thus, it would follow that the net charge of the bZIP peptide N-terminal to DNA determines the magnitude and direction of induced DNA bending. To test this notion, we created a further series of six MBP-bZIP fusion peptides in which the electrostatic character of the linker domain was varied widely (final six entries in Table 1). We observed that dimeric MBP-bZIP fusion peptides containing a total of 20 cationic lysines (10 per monomer) near DNA induced strong DNA bending toward the minor groove, while dimeric peptides with a total of 20 anionic glutamates inverted the shape of DNA in the complex, bending the DNA toward the major groove. These results are consistent with an electrostatic collapse model of DNA bending.

Representative electrophoretic phasing data are shown in Figure 4A. Lanes 1−5 display the mobilities of complexes involving the binding of MBP-PAA to the phasing probes. The introduction of 10 lysine residues to the linker region of MBP-PAA (MBP-K_{10}-PAA; Table 1) dramatically alters the electrophoretic mobility of the DNA phasing probes (Figure 4A, lanes 6−10). Whereas in complexes with MBP-PAA mobility retardation is maximal for probe pDP-AP-1-26 (Figure 4A, lane 3), in complexes with MBP-K_{10}-PAA, mobility retardation is minimal for probe pDP-AP-1-26 (Figure 4A, lane 8) and maximal for probes pDP-AP-1-21 and -30 (Figure 4A, lanes 6 and 10). This result indicates an apparent inversion in the direction of DNA bending induced by the bound protein, with the cationic linker now inducing apparent DNA bending toward the minor groove (Figure 1). An N-terminal shift of this oligo(lysine) sequence was effected by construction of the variant MBP-$K_{10}(GS)_5$-PAA (Table 1). As observed with MBP-K_{10}-PAA, binding of MBP-$K_{10}(GS)_5$-PAA caused apparent DNA bending toward the minor groove (Figure 4A, compare lanes 31−35 to lanes 1−5 and lanes 6−10). Subtle differences in bend orientation were noted between MBP-K_{10}-PAA and MBP-$K_{10}(GS)_5$-PAA. Probes pDP-AP-1-23 and pDP-AP-1-26 appeared to have equal mobilities when bound by MBP-$K_{10}(GS)_5$-PAA (Figure 4A, lanes 32 and 33).

Binding of the anionic variant MBP-E_{10}-PAA (Table 1) enhanced apparent DNA bending toward the major groove relative to MBP-PAA (Figure 4A, lanes 11−15). The overall mobilities of complexes involving MBP-E_{10}-PAA were reduced, suggesting the possibility of a global difference in protein structure, in addition to the DNA bending effect. It is worth noting that simple net charge calculations would

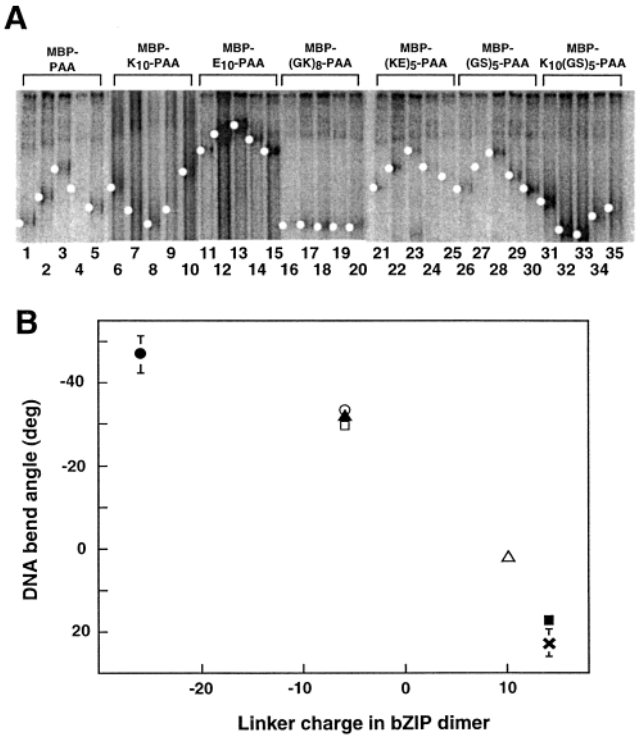

FIGURE 4: Relationship between apparent DNA bend angle and linker charge in the bZIP dimer. (A) Electrophoretic mobility shift assay of MBP-bZIP linker charge variants bound to phasing analysis probes. Each set of five lanes shows phasing probes, as in Figure 2A, incubated with the indicated MBP-bZIP fusions (see Table 1 for designations). Shifted species are highlighted by white dots. (B) Relation between DNA apparent bend angle (see legend to Figure 3) and formal charge in the peptide linker of bZIP dimers. Here, the peptide linker is defined as all residues shown in the body of Table 1, except the MBP domain. Data are plotted as the mean and standard deviation of at least two independent experiments. Error bars are not shown when smaller than the symbols used. Symbols shown represent data for MBP-PAA (open circle), MBP-K_{10}-PAA (filled square), MBP-E_{10}-PAA (filled circle), MBP-$(GK)_8$-PAA (open triangle), MBP-$(KE)_5$-PAA (open square), MBP-$(GS)_5$-PAA (filled triangle), and MBP-$K_{10}(GS)_5$-PAA (cross).

predict an increase rather than a decrease in the relative mobility of complexes with MBP-E_{10}-PAA. Binding of the less cationic variant, MBP-$(GK)_8$-PAA, totally eliminated mobility differences among complexes (Figure 4A, lanes 16−20). This suggests that, in the context of an MBP fusion, the presence of eight lysine residues in the linker domain balances the electrostatic environment near DNA, eliminating induced bending. The electrophoretic equivalence of these complexes (Figure 4A, lanes 16−20) also suggests that protein structure is not being detected in such phasing assays.

Several neutral peptide linker domains of similar length were constructed as controls (Table 1). Introduction of the electrostatically balanced linker variants MBP-$(KE)_5$-PAA and MBP-$(GS)_5$-PAA had no detectable effect on the electrophoretic mobility of bound DNA phasing probes relative to MBP-PAA (Figure 4A, compare lanes 21−25 and 26−30 to lanes 1−5). This result again demonstrates that it is formal charge rather than peptide length or structure that correlates with DNA bending.

The gel mobility measurements for MBP-bZIP fusion variants such as those shown in Figure 4A were again transformed into apparent DNA bend angles as described above. The results were then plotted against the formal dimer charge of the entire linker domain separating MBP and the bZIP domain of GCN4 (Figure 4B). As before, a striking direct relationship is revealed between apparent induced DNA bending and the electrostatic character of the linker domain near DNA. Addition of anionic residues enhanced DNA bending toward the major groove, while the addition of cationic amino acids reversed the direction of bending. Substitution with neutral amino acids did not detectably affect apparent DNA bending.

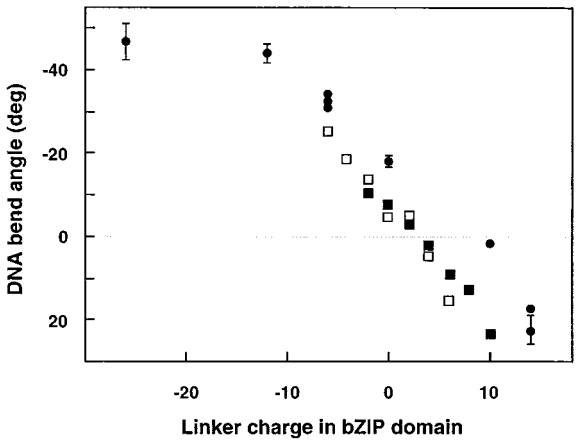

FIGURE 5: Global effect of bZIP N-terminal linker charge on DNA bending. Shown is the relationship between apparent DNA bend angle (see legend to Figure 3) and the formal charge of linker amino acids in bound dimeric bZIP proteins. The peptide linker is again defined as all residues shown in the body of Table 1, except the MBP domain. Symbols shown represent data for T7-XXX peptides (open squares), His-XXX peptides (closed squares), and MBP-bZIP fusion peptides (closed circles). Data are plotted as the mean and standard deviation of at least two independent experiments. Error bars are not shown when smaller than the symbols used.

To compare globally all of our electrophoretic phasing data for bZIP variants, we calculated the net formal dimer charge for the N-termini (or linker domains) of all peptides tested. These charges reflect the amino acids held closest to DNA and most likely to exert minimally screened electrostatic forces on the DNA backbone. Formal N-terminal charges in this region are shown in the right column of Table 1. The summary data are shown in Figure 5. A remarkably strong and consistent dependence of apparent DNA bending on the local protein charge is revealed by this analysis. The magnitude of apparent DNA bending is independent of the structure of the protein, as MBP-bZIP fusion peptides (approximately 5-fold larger than the T7-XXX and His-XXX peptides) induce charge-dependent apparent DNA bend angles consistent with other peptides. This summary analysis reduces concern that protein structure is the basis for charge-dependent electrophoretic anomalies in the absence of DNA bending. In all cases, both the magnitude and direction of the apparent DNA bend angle are strongly dependent on the local electrostatic character of the bound peptide. Moreover, the direction of bending (toward the major or minor groove) is exactly as predicted by a charge-collapse model. The modest rightward displacement of MBP-bZIP data in Figure 5 allows the possibility that additional charge or steric effects of the MBP domains themselves might favor minor groove bending slightly beyond what is suggested by linker charge alone. MBP does carry a net negative charge, though presumably held at a greater distance from DNA.

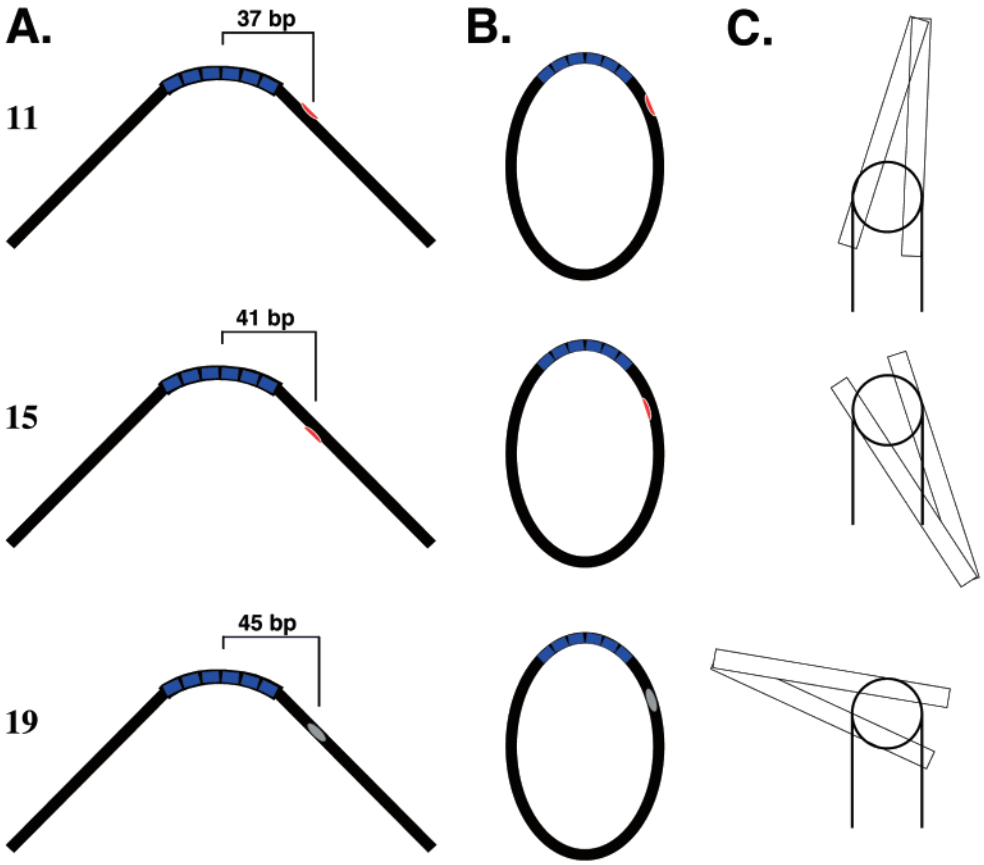

FIGURE 6: Minicircle binding templates. (A) Linear probes: **11** (top), **15** (middle), and **19** (bottom). A_6 tracts are indicated in blue. The AP-1 site is represented as a red oval (gray when facing away from the viewer). The bracket marks the spacing between the A_6 tract array and the AP-1 site. (B) Circular probes: **11** (top), **15** (middle), and **19** (bottom). (C) Model of His-PAA bound to circular probes. The view is end-on, through a virtual section of the AP-1 site.

Minicircle Competition Binding Experiments. We sought to corroborate electrophoretic phasing measurements of apparent DNA bending using independent minicircle competition binding assays. If a protein induces a static bend in its DNA-binding site, the protein may preferentially bind to a circular DNA when the protein binding site is properly phased (e.g., facing inside vs outside of circle), as defined by an array of A_{5-6} tracts in the circle (*15*). Preferential binding to circular DNA is favored if protein binding reduces the free energy of the remaining unbound DNA in the circle. Minicircle binding preferences have been experimentally observed for proteins that induce large DNA bends, such as the TATA box binding protein (*23*) and CAP (*24*). Thermodynamic arguments relate experimental or calculated *J* factors (relative end concentrations) for protein-bound linear DNAs to expected minicircle binding preferences (*24*). In the case of CAP, properly phased minicircles were ~160-fold more effective binding competitors relative to linear DNA, and CAP binding enhanced the *J* factor by a similar factor of ~120-fold (*24*). Related cyclization experiments have measured *J* factors sensitive to the DNA curvature intrinsic to a single A_6 tract (~18°; *15*) and an ~8° bend intrinsic to the ATF/CREB site (*36*). This result implies that modest protein-induced DNA bends should also be detectable in minicircle competition binding assays. This remains to be validated experimentally, and dynamic features of modest protein-induced DNA bends detected in minicircle DNA-binding experiments may differ in subtle but important ways from intrinsic DNA curvature detected in DNA cyclization experiments.

On the basis of previous studies by Crothers and coworkers (*15*), we prepared a set of three radiolabeled 156 bp DNA molecules in linear (Figure 6A) and circular (Figure 6B) forms. Figure 6C displays the different predicted orientations of bound bZIP domains as viewed through a section of the AP-1 site.

We used Monte Carlo simulations to predict the binding preferences to linear vs circular DNA for proteins that bend DNA by 20° into the major or minor grooves of the AP-1 site. The methods used were similar to those previously applied in the analysis of CAP-induced DNA bending (*29*). For A-tract bending we used the junction model, with an A-tract bend of 18°; a wedge model scaled to give the same bend angle gave similar results. Putative protein-induced bending (by roll) was split in half on each side of the central bp of the AP-1 site. No allowance was made for protein-induced stiffening. The lowest energy structure for each construct was generated by simulating an infinitely stiff chain with static bend parameters above. The *J* factors (effective local DNA end concentrations) were computed as described (*29*), and the ratios of *J* factors gave predicted K_{rel} values. The rank order of predicted *J* factors (and corresponding minicircle binding preferences) corresponded well with visual inspection of the lowest energy structures. On the basis of electrophoretic results, our models assumed that His-EEE would induce a 20° major groove bend while His-KKK would induce a 20° minor groove bend (*10*). The predicted

Table 2: Comparison of Predicted and Observed Minicircle Binding Preferences

bZIP charge variant	DNA template	K_{rel}[a] predicted[b]	K_{rel}[a] observed[c]
His-EEE	11	3.7 ± 1.1	1.0 ± 0.2
	15	0.6 ± 0.2	0.9 ± 0.2
	19	1.2 ± 0.4	1.0 ± 0.2
His-KKK	11	0.5 + 0.2	1.0 ± 0.2
	15	2.2 ± 0.7	1.1 ± 0.1
	19	0.7 ± 0.2	0.8 ± 0.1
MBP-KKK	11		0.8 ± 0.3
	15		0.4 ± 0.3
	19		0.4 ± 0.3
MBP-E_{10}-PAA	11		1.1 ± 0.2
	15		0.6 ± 0.2
	19		0.5 ± 0.2

[a] Relative equilibrium binding preference for linear vs circular DNA, as described in eq 1 of Materials and Methods. A K_{rel} value less than 1.0 reflects preferential circle binding. [b] Based on Monte Carlo simulations as described in Materials and Methods. Simulations assumed a bend angle of 20°. [c] Mean ± standard deviation from six (His-peptide) or three (MBP-bZIP) determinations.

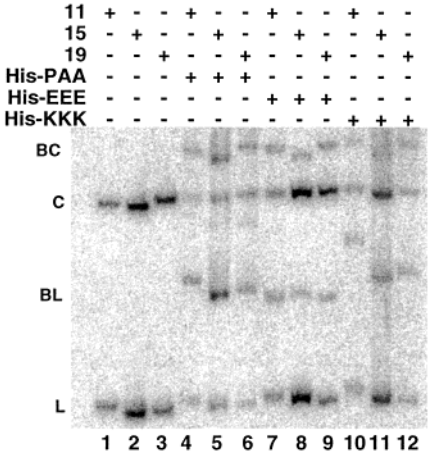

FIGURE 7: Observed minicircle binding preferences of His-XXX peptides. Each set of three lanes contains both linear and circular forms of binding probes **11**, **15**, and **19**, respectively, incubated with subsaturating amounts of purified His-PAA (lanes 4−6), His-EEE (lanes 7−9), and His-KKK (lanes 10−12). Samples in lanes 1−3 contained no protein. Free (L) and bound (BL) linear probes and free (C) and bound (BC) circular probes are indicated.

binding preferences are displayed in Table 2. Although modest, distinct binding preferences are predicted by theory. As K_{rel} describes the relative preference for binding to linear vs circular DNA, values less than 1.0 reflect preferential circle binding. For binding of His-EEE, the circular form of **15** is predicted to be bound 2-fold more tightly than the linear form of **15**. His-KKK is predicted to bind circular **11** 2-fold more tightly than the linear form of **11**. Minicircle **19** was predicted to be intermediate in binding preference. More significant are differences among K_{rel} values within a given set of peptide complexes. Simulations predict maximal differences among K_{rel} values in both His-EEE and His-KKK complexes to approach 5-fold.

Example data from minicircle competition binding assays are presented in Figure 7. Linear and circular forms of probes **11**, **15**, and **19** migrate distinctly when electrophoresed through native polyacrylamide gels (Figure 7, lanes 1−3). These probes were then assembled with subsaturating concentrations of peptide added to binding reactions. Preliminary order-of-addition experiments showed that binding equilibrium had been reached (data not shown). We first tested His-PAA (Figure 7, lanes 4−6). No differential binding preferences for circular vs linear DNA were observed. We then tested the charge variants His-EEE (Figure 7, lanes 7−9) and His-KKK (Figure 7, lanes 10−12). Despite the prediction of significant variation among K_{rel} values, no significant binding preferences for circular vs linear DNAs were observed (Table 2). Similar results were obtained for MBP-bZIP fusion proteins (Table 2).

DISCUSSION

We confirm with an extensive series of bZIP peptides that variations in amino acid charge near the DNA cause phase-dependent alterations in gel mobility. As shown in Figure 5, a remarkably strong and consistent dependence of apparent DNA bending on the local protein charge is observed, as in our previous studies (*10*). The magnitude of apparent DNA bending is independent of the size and structure of the engineered bZIP protein. The consistency of these results clearly reduces concern regarding the potential of protein structure to cause charge-dependent electrophoretic anomalies in the absence of DNA bending. In all cases, both the magnitude and direction of the apparent DNA bend angle are strongly dependent on the local charge of the bound peptide. The greater the cationic character of the linker N-terminal to the bZIP domain, the greater the apparent collapse of the DNA toward that cationic locus (minor groove bending, away from the leucine zipper). On the other hand, as predicted, the presence of anionic amino acids N-terminal to the DNA is accompanied by greater apparent DNA bending away from the anionic locus (major groove bending, toward the leucine zipper). Despite this remarkable and persistent correlation of peptide charge with apparent DNA bend magnitude and direction in electrophoretic phasing assays, we report that DNA bending by engineered bZIP charge variants is not detected in minicircle binding assays. Similar discrepancies have been noted previously (*15*). We believe that the case for a dominant electrostatic consideration in DNA bending is nonetheless strengthened by (i) our observation of a persistent correlation between apparent DNA bending and local peptide charge and (ii) the independence of this result from peptide structure.

Local Electrostatic Effects. In our calculation of local peptide charge, we have chosen to consider only the linker amino acids near DNA, due to ion screening considerations. Polyelectrolyte theory suggests that, at the ionic strength of our electrophoresis conditions, amino acid charges are unscreened and interact fully with DNA phosphates if within ~7.5 Å of DNA (*37*). On the other hand, electrostatic interactions are predicted to be screened fully beyond 40 Å. Between 7.5 and 20 Å, a more complex situation is predicted, as approaching charges interact more with condensed counterions than DNA phosphates. As a consequence, electrostatic forces may actually be inverted (*38*). However, in all cases Coulombic forces scale as $1/r^2$, where r is the charge separation. These considerations confirm that amino acids very near DNA should dominate in terms of electrostatic bending forces. Because the molecular geometries of the various linker domains are unknown, our calculations weight all formal charges equally. For the reasons listed above, this is an extreme simplification. Because cationic amino acids

show similar DNA bending effects in MBP-K_{10}-PAA and MBP-K_{10}-$(GS)_5$-PAA, the neutral spacer does not appear to move the cationic domain substantially farther from the DNA. Others have invoked electrostatic effects over even longer distances to explain protein effects on DNA shape (*21*). Phasing-independent global changes in gel mobility (e.g., MBP-E_{10}-PAA; Figure 4A, lanes 11−15) do suggest that overall protein structures may differ in some charge variants. Such effects do not nullify the implication of phasing-dependent mobility changes. We note that our conclusions do not change when we count formal charges of all bZIP amino acids on both sides of the DNA (i.e., including charges in the leucine zipper; data not shown).

bZIP Geometry. Our studies were motivated, in part, by concern that some aspect of the asymmetric geometry of the leucine zipper domains of bZIP proteins causes phase- and charge-dependent gel mobility differences that have been misinterpreted as DNA bending. Such reasoning predicts that, in the absence of induced DNA bending, the different orientations of bound bZIP proteins on phasing probes would produce slow "Y-shaped" (zipper and A tract curvature extend in opposite directions) vs fast "F-shaped" (zipper and A tract curvature extend in the same direction) isoforms (*15*). However, our peptide constructs behave in opposition to what would be predicted if the Y-shaped vs F-shaped DNA−protein complex model is invoked to explain gel mobility anomaly in the absence of DNA bending. First, cases such as T7-PAA show little phase-dependent difference in gel mobility, despite radical changes in orientation of the zipper through all geometries, including Y-shaped and F-shaped (*10*). Second, it is typically reasoned that F-shaped geometries should migrate more quickly than Y-shaped geometries. For T7-PAA, His-PAA, and MBP-PAA, we observe the opposite trend, with F-shaped complexes running more slowly through gels.

Other arguments have attributed gel mobility anomaly to differential flexibility of the protein−DNA interface (*15*). It has been suggested that, at low ionic strength, electrostatic interactions in the basic region of Fos-Jun may rigidify the leucine zipper relative to the DNA helix, causing shape-dependent phasing effects that are misinterpreted as DNA bending (*15*). While it is possible that our bZIP fusions may have differential flexibilities when bound to DNA, we feel it is unlikely that this contributes to the observed charge-dependent electrophoretic mobility differences. If bZIP proteins bind flexibly in the absence of a charged framework, the absence of phasing effects for T7-PAA and His-PAA implies that flexible complexes do not mimic DNA bending. If cationic substitutions induce leucine zipper rigidification without DNA bending, we must conclude that such rigidification mimics an apparent DNA bend toward the minor groove. However, one must then assume that substitution with anionic residues somehow inverts this effect to mimic DNA bending toward the major groove. If anionic variants simply have more zipper flexibility than neutrals, it seems more likely that enhanced flexibility would minimize, not enhance, differences among phasing probe mobilities. Finally, the above zipper flexibility argument would need to dominate even in bZIP fusions to MBP, where the protein structure is no longer asymmetric.

Minicircle Binding Assays. We were motivated to corroborate our electrophoretic phasing assay data with an independent, solution-based DNA bending assay. Minicircle binding competition assays have previously been suggested for this purpose. We show that these assays do not detect minicircle binding preferences predicted from our electrophoretic results. Several points regarding the minicircle assay and this apparent discrepancy deserve further consideration.

First, it is possible that the minicircle competition assay is insensitive to the small apparent DNA bend angles induced by the binding of the studied family of bZIP derivatives. To date, calibration experiments in the minicircle format have been limited to proteins that bend DNA strongly. Experiments with CAP established a quasi-thermodynamic cycle linking cyclization enhancement and preferential binding to proper circular substrates (*24*). This work suggested that the ratio of minicircle binding preference to *J* factor enhancement is in the range of 1.3−3.3-fold. While cyclization rate studies have been shown to be sensitive to small DNA bends (*36*), this result has not been confirmed in the format of minicircle binding competition assays.

Second, we used Monte Carlo simulations to predict that minicircle binding preferences with two of our studied bZIP derivatives might be detectably different. However, differences of only 2−3-fold were predicted, leaving open the possibility that details of the DNA probe size and the phasing between the GCN4 binding site and phased A_6 tracts diminish the sensitivity of the assay to GCN4-induced bends. Examination of cyclized DNA chains from our Monte Carlo simulations suggests that the closed circular molecules are oval-shaped, and since the AP-1 site is near the highly bent A tracts, the site tends to be straight, reducing the effect one would expect. Consideration of this "bend focusing" effect in the design of minicircle constructs might improve their sensitivity.

We propose a unifying interpretation that reconciles many of the apparently disparate results in this area. There are two puzzling issues: (1) bZIP proteins appear bent in electrophoretic and fluorescence resonance energy transfer (FRET) assays (*25*) but not in cyclization or minicircle binding assays. (2) bZIP protein variants which induce different apparent extents of binding appear to bind with similar affinities. This second puzzle suggests the surprising conclusion that somehow the stabilities of the protein−DNA complexes can be independent of their DNA strain energies. For this to be true, it suggests that the less deformed protein−DNA complexes have counterbalancing free energy costs associated with them, perhaps deformation of the protein or decreased/suboptimal ionic interactions. Given the idea that very similar proteins adopt rather different geometries, we think it reasonable to suggest that an individual protein−DNA complex can similarly adopt a range of geometries. In this case, we expect that as a highly bent complex straightens, the loss of DNA strain energy is balanced by a free energy cost from lost ionic interactions. Thus, we proposed that the charge collapse model of bending predicts a relatively flat potential surface for bending.

Connecting this idea back to puzzle 1 above, we propose that the electrophoretic, FRET (*25*), and cyclization assays may be sampling different parts of the bending potential surface (Figure 8). The electrophoretic and FRET methods are presumably sensitive to an average conformation. In contrast, the minicircle binding/cyclization experiment selects out the part of the population that allows for efficient

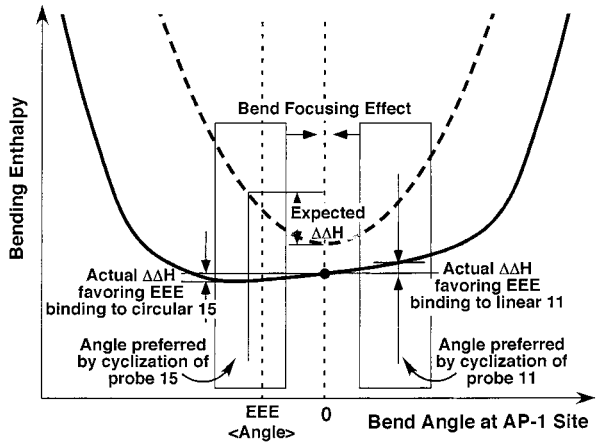

FIGURE 8: The energy diagram sketches the proposed cause for the observed lack of discrimination among bent DNAs in minicircle binding assays. The dashed curve schematically represents the bending enthalpy potential for normal DNA, and the solid curve represents a hypothetical bending potential for the His-EEE−DNA complex. The expected bending free energy change upon binding a bending protein to a circle depends on the free energy benefit to be expected from prebending free DNA and minimizing strain in the remainder of the DNA molecule. However, a hyperflexible protein−DNA bend might adapt to a range of minicircle geometries, so that minicircle binding selects out a restricted set of available conformations, as indicated by the boxes. The consequent entropy cost compensates for the gain in binding enthalpy obtained from prebending, and the energy difference for adapting to any geometry required by the minicircle is small, hence the lack of preferential binding to circle vs linear or to one circle vs another. The flat potential is proposed to be due to competing interactions in the peptide−DNA complexes, such that increased DNA bending strain is balanced by favorable protein−protein interactions and the total free energy is relatively independent of bend angle. The His-KKK complex potential would be inverted right to left. The bend focusing effect refers to the idea that the minicircles used here may actually constrain the AP-1 site to a fairly straight geometry, accessible to any of the peptide−DNA complexes. A minicircle geometry that constrained the AP-1 site to a more bent shape might show stronger preferences for asymmetrically flexible protein−DNA complexes.

cyclization. If all of the complexes are sufficiently flexible to adapt to a range of minicircle closure constraints, then they will not be distinguishable in minicircle assays. A minicircle that required significant bending in the AP-1 site might be expected to favor binding of a highly bent peptide, but this will be counterbalanced by a loss of entropy in the protein−DNA conformation upon binding to a minicircle relative to a linear DNA. Finally, this interpretation suggests that it may be the adaptability of bZIP transcription factors to different geometries, rather than a specific induced structure, that allows them to function in a variety of transcription activation complexes. It remains to be seen whether bZIP charge variants are exceptional relative to other DNA bending proteins in this regard.

CONCLUSIONS

The experiments described here suggest three conclusions. First, we believe that our results add support to the view that local protein charge can strongly influence DNA shape in the protein−DNA complex under electrophoretic conditions. Second, our data support the general reliability of electrophoretic phasing assays of DNA shape, even for small asymmetric proteins such as bZIP dimers. Third, certain proteins that modestly bend DNA may not yield consistent results in different bending assays. Representatives of the peptide constructs investigated here showed DNA bending by electrophoretic phasing and FRET assays (*25*) but not by minicircle binding assays.

ACKNOWLEDGMENT

We thank Ayesha Sitlani, Don Crothers, and Alanna Schepartz for materials, helpful discussion, and assistance. We also thank Tom Kerppola and Gerald Manning for helpful discussion.

REFERENCES

1. Luger, K., Mader, A. W., Richmond, R. K., Sargent, D. F., and Richmond, T. J. (1997) *Nature 389*, 251−260.
2. Parkinson, G., Wilson, C., Gunasekera, A., Ebright, Y. W., Ebright, R. E., and Berman, H. M. (1996) *J. Mol. Biol. 260*, 395−408.
3. Goodman, S. D., and Nash, H. A. (1989) *Nature 341*, 251−254.
4. Kahn, J. D., and Crothers, D. M. (1993) in *Cold Spring Harbor Symposia on Quantitative Biology*, pp 115−122, Cold Spring Harbor Laboratory Press, Cold Spring Harbor, NY.
5. Maher, L. J. (1998) *Curr. Opin. Chem. Biol. 2*, 688−694.
6. Mirzabekov, A. D., and Rich, A. (1979) *Proc. Natl. Acad. Sci. U.S.A. 76*, 1118−1121.
7. Manning, G. S., Ebralidse, K. K., Mirzabekov, A. D., and Rich, A. (1989) *J. Biomol. Struct. Dyn. 6*, 877−889.
8. Strauss, J. K., and Maher, L. J. (1994) *Science 266*, 1829−1834.
9. Strauss, J. K., Roberts, C., Nelson, M. G., Switzer, C., and Maher, L. J. (1996) *Proc. Natl. Acad. Sci. U.S.A. 93*, 9515−9520.
10. Strauss-Soukup, J., and Maher, L. J. (1998) *Biochemistry 37*, 1060−1066.
11. Williams, L. D., and Maher, L. J. (2000) *Annu. Rev. Biophys. Biomol. Struct. 29*, 497−521.
12. Strauss-Soukup, J. K., and Maher, L. J. (1997) *Biochemistry 36*, 10026−10032.
13. Kerppola, T. K., and Curran, T. (1993) *Mol. Cell. Biol. 13*, 5479−5489.
14. Paolella, D. N., Liu, Y., and Schepartz, A. (1997) *Biochemistry 36*, 10033−10038.
15. Sitlani, A., and Crothers, D. (1998) *Proc. Natl. Acad. Sci. U.S.A. 95*, 1404−1409.
16. Ellenberger, T. E., Brandl, C. J., Struhl, K., and Harrison, S. C. (1992) *Cell 71*, 1223−1237.
17. Kerppola, T. K., and Curran, T. (1991) *Cell 66*, 317−326.
18. Crothers, D. M., and Drak, J. (1992) *Methods Enzymol. 212*, 46−71.
19. Sitlani, A., and Crothers, D. M. (1996) *Proc. Natl. Acad. Sci. U.S.A. 93*, 3248−3252.
20. Kerppola, T. K. (1996) *Proc. Natl. Acad. Sci. U.S.A. 93*, 10117−10112.
21. Kerppola, T. K., and Curran, T. (1997) *EMBO J. 16*, 2907−2916.
22. Hagerman, P. J. (1996) *Proc. Natl. Acad. Sci. U.S.A. 93*, 9993−9996.
23. Parvin, J. D., McCormick, R. J., Sharp, P. A., and Fisher, D. E. (1995) *Nature 373*, 724−727.
24. Kahn, J. D., and Crothers, D. M. (1992) *Proc. Natl. Acad. Sci. U.S.A. 89*, 6343−6347.
25. Hardwidge, P. R., Williams, S. L., Wu, J., Parkhurst, K. M., Parkhurst, L. J., and Maher, L. J. (2002) *Biochemistry* (in press).
26. Paolella, D. N., Palmer, C. R., and Schepartz, A. (1994) *Science 264*, 1130−1133.
27. Thompson, J. F., and Landy, A. (1988) *Nucleic Acids Res. 16*, 9687−9705.
28. Kerppola, T. K. (1994) in *Transcription: mechanisms and regulation* (Conaway, R. C., and Conaway, J. W., Eds.) pp 387−424, Raven Press, New York.
29. Kahn, J. D., and Crothers, D. M. (1998) *J. Mol. Biol. 276*, 287−309.
30. Koo, H. S., Drak, J., Rice, J. A., and Crothers, D. M. (1990) *Biochemistry 29*, 4227−4234.

31. Levene, S. D., and Crothers, D. M. (1986) *J. Mol. Biol. 189*, 61−72.
32. Bolshoy, A., McNamara, P., Harrington, R. E., and Trifonov, E. N. (1991) *Proc. Natl. Acad. Sci. U.S.A. 88*, 2312−2316.
33. Hardwidge, P. R., Zimmerman, J. M., and Maher, L. J. (2000) *Nucleic Acids Res. 28*, e102.
34. McCormick, R. J., Badalian, T., and Fisher, D. E. (1996) *Proc. Natl. Acad. Sci. U.S.A. 93*, 14434−14439.
35. Sharff, A. J., Rodseth, L. E., Szmelcman, S., Hofnung, M., and Quiocho, F. A. (1995) *J. Mol. Biol. 246*, 8−13.
36. Hockings, S. C., Kahn, J. D., and Crothers, D. M. (1998) *Proc. Natl. Acad. Sci. U.S.A. 95*, 1410−1415.
37. Cantor, C. R., and Schimmel, P. R. (1980) *Biophysical chemistry part III: The behavior of biological macromolecules*, W. H. Freeman, New York.
38. Manning, G. S., and Ray, J. (1999) *J. Biomol. Struct. Dyn. 16*, 461−476.

BI020185H